Reactive Molecular Dynamics Simulations of Shock Through a Single Crystal of Pentaerythritol Tetranitrate

Joanne Budzien,*,† Aidan P. Thompson,† and Sergey V. Zybin‡

Sandia National Laboratories, Albuquerque, New Mexico 87185, and California Institute of Technology, Pasadena, California 91125

Received: February 23, 2009; Revised Manuscript Received: June 30, 2009

Large-scale molecular dynamics simulations and the reactive force field ReaxFF were used to study shock-induced initiation in crystalline pentaerythritol tetranitrate (PETN). In the calculations, a PETN single crystal was impacted against a wall, driving a shockwave back through the crystal in the [100] direction. Two impact speeds (4 and 3 km/s) were used to compare strong and moderate shock behavior. The primary difference between the two shock strengths is the time required to exhibit the same qualitative behaviors with the lower impact speed lagging behind the faster impact speed. For both systems, the shock velocity exhibits an initial deceleration due to onset of endothermic reactions followed by acceleration due to the onset of exothermic reactions. At long times, the shock velocity reaches a steady value. After the initial deceleration period, peaks are observed in the profiles of the density and axial stress with the strongly shocked system having sharp peaks while the weakly shocked system developed broad peaks due to the slower shock velocity acceleration. The dominant initiation reactions in both systems lead to the formation of NO_2 with lesser quantities of NO_3 and formaldehyde also produced.

1. Introduction

Pentaerythritol tetranitrate (PETN) is a commonly used high explosive (HE) with chemical formula ($C_5H_8N_4O_{12}$) [see Figure 1]. One of the unusual properties of PETN is that shock sensitivity depends on crystal orientation. PETN has a tetragonal crystal structure with two molecules per unit cell, and the directional sensitivity has been attributed to activation of different slip systems when compressing along different crystal axes.[1,2] Experiments have shown that the [110] direction is significantly more sensitive than the [100] direction, with detonation in the [100] direction requiring pressures approximately equal to the Chapman−Jouguet pressure.[3]

In his landmark experiment on a single crystal of PETN, Dick[4] demonstrated a significant influence of the mechanical effects associated with shock compression on the sensitivity. However, a complete understanding of how those phenomena lead to detonation is still missing. The lack of an atomic-level understanding of the basic physical and chemical processes that dominate initiation has also hindered the elucidation of interactions between external shock, material structure, and molecular properties. A substantial amount of effort has been expended in the development of experimental techniques to study these processes; however, those experimental studies have not yet provided satisfactory explanations of the initial steps of detonation.

Molecular dynamics simulation (MD) is a powerful tool that can be used to examine physical and chemical changes occurring at the atomic scale. Developing predictive models of the initiation of detonation and the sensitivity of high explosives demands the large-scale coupling of both chemistry and physics in the simulations. In this work, we use the first-principles-
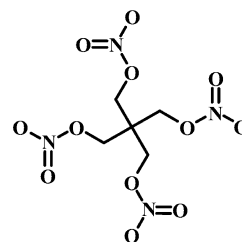

Figure 1. Schematic of a PETN molecule.

based reactive force field ReaxFF,[5,6] which is capable of simulating chemical reactions that occur during dynamical processes associated with various conditions, including high pressures and temperatures. This approach allows atomistic simulations of reactive processes in systems composed of millions of atoms.[7]

By using nonequilibrium MD to study the effect of shock-waves propagating through a perfect crystal of PETN, we were able to track the initiation of chemical reactions behind the shock front to elucidate the coupling between chemical energy release and changes in physical distributions of pressure and temperature fields. These changes are expected to lead to acceleration of the shock front and the transition to detonation.

Due to the large computational cost of performing MD using forces obtained from quantum electronic structure calculations, previous simulations investigating reactions due to high energy collisions of PETN molecules have generally been composed of just two colliding molecules.[8,9] Our simulations are much larger with a cross-sectional area of 4 × 4 unit cells, a length of at least 256 unit cells up to a maximum of 504 cells in some runs and a total atom count varying from 237 568 to 467 712. These large systems enable us to examine correlated reactions and product distributions in ways that are impossible to do using only binary collisions and the very small system simulations in previously published work.[8−10]

---

* Author to whom correspondence should be addressed. Currently at Frostburg State University. E-mail: jbudzien@frostburg.edu.
† Sandia National Laboratories.
‡ California Institute of Technology.

Shock Through a Single Crystal of PETN

J. Phys. Chem. B, Vol. 113, No. 40, 2009 **13143**

In this work, the PETN crystal was shocked by ramming it against a repulsive wall at speeds of 3 km/s (weak shock) and 4 km/s (strong shock). In initial tests, these two different impact speeds were identified as leading to shock velocities that bracket the experimental detonation velocity. This results in being able to observe both slow and fast decomposition rates.

In both cases, the resultant shock front velocity was found to vary as a function of time. The shock front in the strongly shocked system initially accelerated and then remained constant, while in the weakly shocked system, the shock front showed an initial slight deceleration followed by a sharp acceleration. Changes in thermodynamic properties were tracked in spatially resolved ways so that profiles of some relevant properties (temperature, axial stress, and density) could be measured as a function of position in the crystal. For all times, the strongly shocked crystal exhibited peaks near the shock front for most of these properties; the weakly shocked crystal only began to develop a broad peak near the shock front at later times.

In addition to examining the differences between the two types of shocks in an attempt to relate atomistic processes to properties that lead to detonation, the chemical reactions themselves are of interest. Of primary interest is determining which bond breaks first during initiation and what reaction pathways are likely to dominate the initiation reactions. To restate the first part of the question, referring again to Figure 1, which moieties are likely to be observed in large quantities: NO_2, ONO_2, or an entire arm of CH_2ONO_2?

To investigate the initiation pathways, chemical reactions were also observed with data for product concentrations examined both as a function of time and as a function of position behind the shock front. NO_2 was observed to be the dominant initial product with NO_3 and HNO_2 formation as the other initiation products produced in large quantities. Formaldehyde was produced in much lower quantities than NO_2, HNO_2, or NO_3. Trace amounts of CH_2NO_3 fragments were also observed.

The rest of this paper is organized in three main sections. The immediately following section details the simulated systems, gives a brief description of the simulation parameters, and describes the analysis methods. The results and discussion section begins by presenting the shock velocities, continues by describing the thermodynamic properties, and concludes with an account of the observed chemical reactions and the resulting products. The final section is a summary of the results.

2. Method

We performed MD simulations of planar shocks in single crystals of PETN using the ReaxFF reactive force field[5] implemented in the GRASP[11] parallel MD code. The crystals were oriented such that the shock would propagate in the [100] direction. The initial systems consisted of 256 unit cells in the shock direction and 4 unit cells in the two directions perpendicular to the shock, leading to a system size of 2440 Å × 39.4 Å × 30.5 Å with 237 568 atoms. Periodic boundary conditions were applied in the direction perpendicular to shock. The direction parallel to shock propagation was not periodic.

To generate a shock, all the atoms in the crystal were given an extra velocity in the negative x-direction, colliding the crystal with a piston, which is represented by a stationary wall. This piston interacts with the system atoms via the Lennard-Jones 9−3 potential:

$$U_{wall} = \frac{2\varepsilon}{15}\left[\left(\frac{\sigma}{r}\right)^9 - \left(\frac{\sigma}{r}\right)^3\right] \quad r \leq r_{cut}$$
$$U_{wall} = 0 \qquad\qquad\qquad r > r_{cut} \tag{1}$$

where r is the distance of an atom from the wall, $\varepsilon = 5.0$ kcal/mol, $\sigma = 3.0$ Å, and $r_{cut} = 7.5$ Å. This procedure is equivalent to driving the wall into an initially stationary crystal with a velocity u_{wall} in the positive x-direction. Two different piston velocities, $u_{wall} = 3.0$ and 4.0 km/s, were used in these simulations. Unfortunately, the nonperiodic boundary condition in the x-direction means that simulation time is limited to the time required for the shock front to travel from the wall to the free surface on the opposite side of the crystal. The reflection of the shockwave at the free surface generates a rarefaction wave that travels back through the crystal, preventing further examination of the shocked state. All the data presented in this paper was collected before the rarefaction wave was generated.

After reviewing the initial results up to the point that the shock front produced a rarefaction wave, we decided to extend the simulations in a way that would not disrupt the shocked material. Taking the configuration for the system of $u_{wall} = 3.0$ km/s at 35 ps (a few picoseconds before the shock front reached the free surface of the crystal), we added a slab of equilibrated crystal on to the end of the existing crystal. We first removed the material within four unit cells of the free surface, which was sufficient to obtain atoms that were at the bulk density. The added atoms were shifted in x (but not in the other two directions) to form a continuous crystal with the remaining uncompressed crystal at 35 ps. The size of the extended system was 2580 Å × 39.4 Å × 30.5 Å with 352 640 atoms. This system was extended again at 50 ps using a similar method to give a final system size of 467 712 atoms with dimensions of 3311 Å × 39.4 Å × 30.5 Å. The 4 km/s system was extended in a similar manner at 25 ps to give dimensions of 2626 Å × 39.4 Å × 30.5 Å with 352 640 atoms.

Systems were thermalized under *NVT* conditions at 300 K for several picoseconds before the shock was applied. The density of the system is 1.47 g/cm^3, which is lower than the experimental single crystal value of 1.77 g/cm^3. This density was obtained by manipulating the simulation box in order to obtain zero pressure. The resulting crystal is no longer exactly tetragonal (unit cell dimensions are 9.5 Å × 9.8 Å × 7.6 Å). The reason for the pressure discrepancy is that ReaxFF has been fit to density functional theory (DFT) calculations, which are known to underestimate the equilibrium density of HE crystals[6] because of difficulties in describing weak van der Waals binding interaction between molecules. Here we use the ReaxFF developed for nitramines,[12] which was extended to triacetone triperoxide[13] and nitromethane[14] and that has been further modified for PETN by additional fitting to DFT data on specific decomposition reactions in PETN and to a cold compression curve.

TABLE 1: List of Bond Order Minimum Values Used to Determine Molecules

atom type	atom type	bond order
C	C	0.55
C	H	0.40
C	N	0.30
C	O	0.65
H	H	0.55
H	N	0.55
H	O	0.40
N	N	0.55
N	O	0.40
O	O	0.65

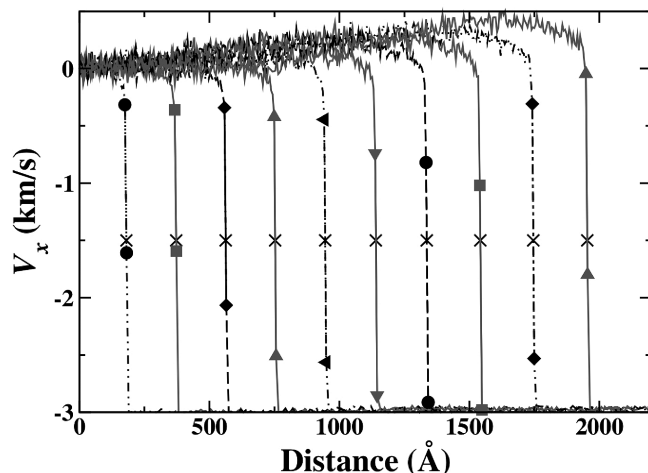**Figure 2.** *x* component of mass velocity for $u_{wall} = 3$ km/s. The symbol × denotes the determined position for the shock front. The curves and associated symbols are times relative to the first strike on the wall in 5 ps intervals from 5 to 50 ps.
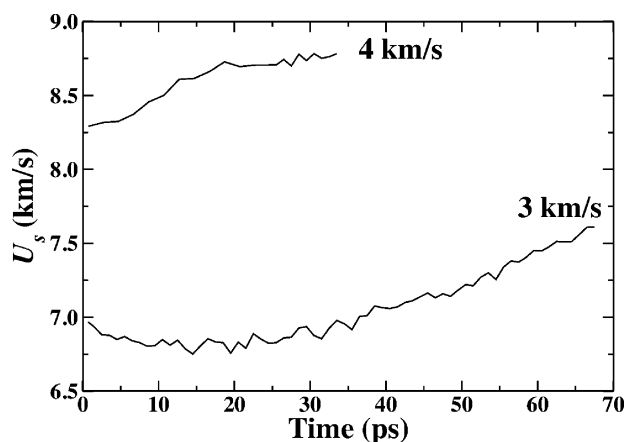

Figure 3. Shock front velocity as a function of time.

Once the systems were thermalized, shock simulations were conducted using *NVE* conditions. In all cases, a time step of 0.1 fs was used. This time-step size was found to adequately conserve energy under *NVE* conditions with chemical reactions that involve bond-breaking processes. The instantaneous charge on each atom was calculated self-consistently every step using the electronegativity equalization method[15,16] with a tolerance of 1.0×10^{-5} or 1.0×10^{-6}.

At regular intervals, spatial profiles of various quantities were generated through a binning procedure. One unit cell of thickness in the shock propagation direction corresponds to 928 atoms. Therefore, quantities were averaged in bins of 928 atoms with the members of each bin determined by *x* coordinate. Each averaged value was then assigned an *x* coordinate based on the geometric average of the *x* coordinate of the atoms in the given bin. While this procedure gives a reasonably sharp shock front (bins tend to span about 10 Å), this fine grid amplifies noise away from the shock front. To decrease the noise resulting from too fine a binning procedure, the binned data away from the shock front is plotted here as a block average of five to ten points, depending on the particular quantity measured.

The primary advantage of using ReaxFF in simulations is the ability to model reactions. Bonding is not fixed during the simulation; instead, bond orders are self-consistently calculated at each step and are used to determine the instantaneous valence force and interaction energy between each atom pair within the

cutoff radius. These relationships are continuous and monotonic with the parameters determined by multiple DFT calculations involving each type of bond breaking process and intermediate state. The bond orders are determined through proximity and the local environment of atom pairs, with minor corrections to help enforce physically reasonable coordination.

To determine molecules in the system, we postprocessed files containing bond orders generated during the simulation. Pairs of atoms that had instantaneous bond orders above the minimum values for the appropriate type of bond (see Table 1) were deemed bonded. In previous ReaxFF simulations,[12−14,17,18] a bond order cutoff of 0.3 for all atom types has been routinely used. However, we found that at high density typical for shock compression the value of 0.3 is too low and leads to a significant number of spurious bonds and clusters. We attempted a cutoff scheme with individual minimum bond orders for each pair of atoms to reflect their covalence. The minimum values given in Table 1 were refined based on identification of common molecules such as PETN, H_2O, CO_2, and N_2 at the initial density of uncompressed PETN. In other words, we chose the largest possible minimum cutoff values that still left those molecules intact. These values are not dependent on density or temperature. Determining bonds by comparison to a minimum bond order may identify spurious bonds in densely packed regions because of the reliance of bond order calculation on proximity. Choosing different minimum values to identify bonds did not eliminate the spurious bonds.

Molecules were identified by considering the connectivity of atoms and counting numbers of each atom type that form a
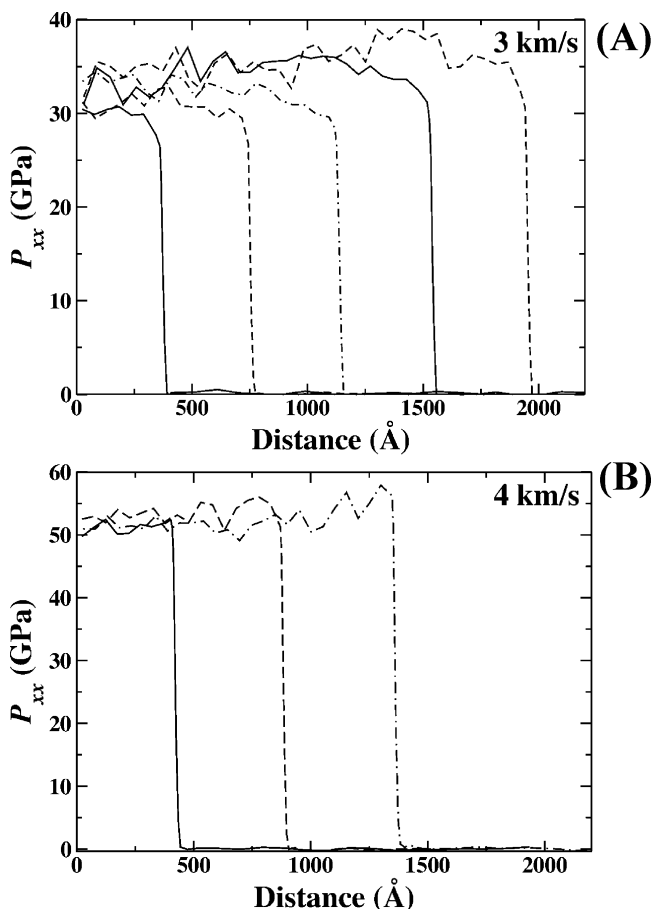

Figure 4. Axial stress. Curves denote ten picosecond intervals beginning with 10 ps on the left and ending with 50 ps (30 ps for $u_{wall} = 4$ km/s) on the right. $u_{wall} =$ (A) 3 and (B) 4 km/s.

Shock Through a Single Crystal of PETN

J. Phys. Chem. B, Vol. 113, No. 40, 2009 **13145**
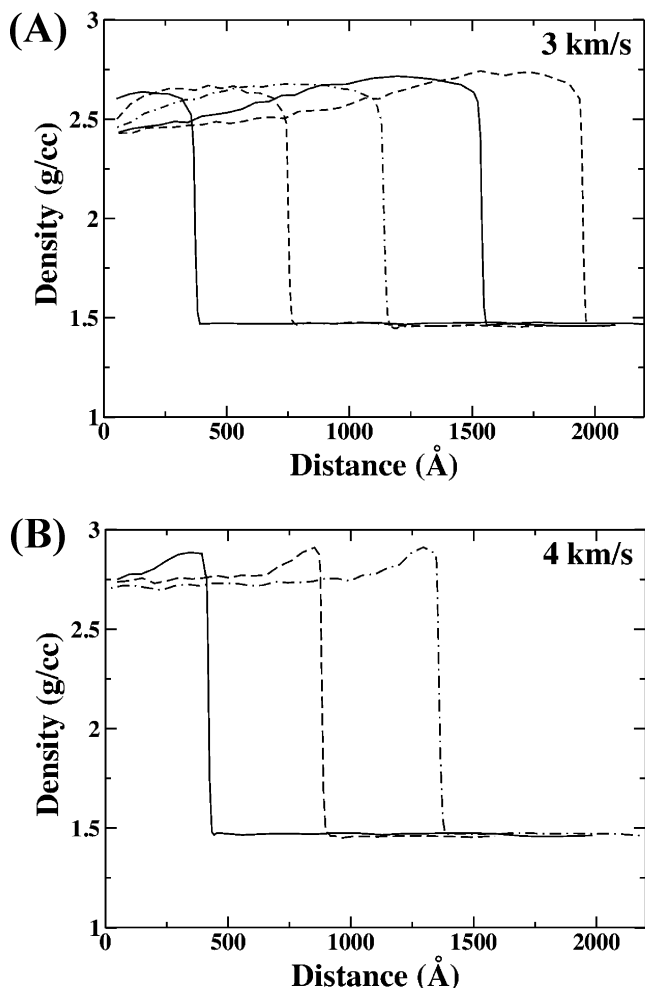
(A)

(B)

Figure 5. Density as a function of position in crystal. Curves denote ten picosecond intervals beginning with 10 ps on the left and ending with 50 ps (30 ps for $u_{wall} = 4$ km/s) on the right. $u_{wall} = $ (A) 3 and (B) 4 km/s.

contiguous cluster. No check was made of molecular topology; all isomers were counted as the same molecule. No attempt was made to correct for spurious bonds, and therefore, some atoms were assigned to large clusters with no effort made to subdivide these clusters into more likely molecules. Doing a molecular analysis on the fly by comparing bond orders averaged over a few time steps instead of the instantaneous method used here may ameliorate the spurious bond issues, but that method is more computationally expensive and was not attempted here.

3. Results and Discussion

To calculate shock front velocities, the positions of the shock front at regular intervals were determined and used to calculate velocities. Short times are 0.1 ps intervals and longer times have 0.01 ps intervals. The position of the shock front was determined from the x component of the velocity. A linear interpolation was used between the two points that bracket the half-maximum velocity (e.g., 1.5 km/s for the 3 km/s piston) to determine the position of the shock front. Examples of the velocity data used and the resulting shock front positions (x_s) are shown in Figure 2. In this work, all spatial profiles are graphed in the frame of the wall located at $x = 0$. The relative shock front velocity ($w(t)$) was then calculated from linear regression on a set of points that span 1 or 2 ps (more frequent positions require fewer points to get a low error slope) and is plotted at the time at the center of the time window.

The shock velocities for the two systems as a function of time are shown in Figure 3. These shock velocities are reported relative to the unshocked PETN crystal so that $U_s = w(t) + u_{wall}$. The shock velocity from the stronger shock appears to be accelerating until it reaches a constant velocity at about 20 ps, while that of the weaker shock appears to be decelerating up to 15 ps, and then, it, too, starts to accelerate, but at a much slower rate. The behavior of the weaker shock is related to considerably slower energy release from the secondary product reactions. A prolonged period of initial NO_2 dissociation, an endothermic reaction, is correlated with the deceleration with the results shown later in this paper during the discussion of chemical reactions.

To compare with experimental values of the detonation velocity, we use the work of Green and Lee,[19] who analyzed a large set of experimental data for PETN at a variety of densities. They found that the data could be fit using the equation

$$D = 3.30 + 3.7(\rho_0 - 0.4) \quad 0.4 < \rho_0 < 1.6 \quad (2)$$

with D as the detonation velocity in kilometers second and ρ_0 as the density in grams per cubic centimeter. This relation yields the velocity of steady detonation wave as 7.26 km/s at our zero-pressure density. From Figure 3, the strongly shocked system has a shock velocity that is always faster than that value, while the weakly shocked system starts below that value and does
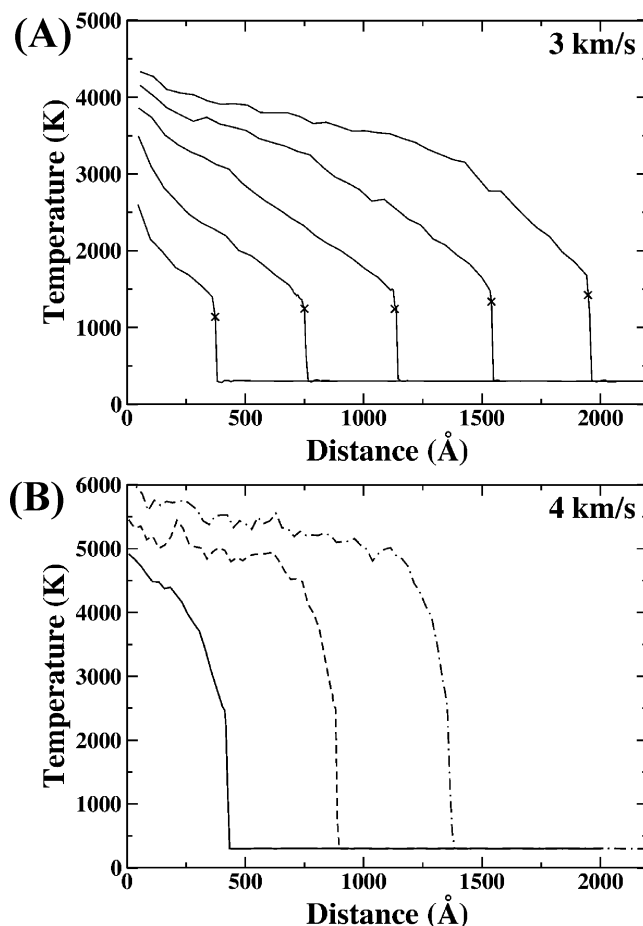
(A)

(B)

Figure 6. Temperature profile. Curves denote ten picosecond intervals beginning with 10 ps on the left and ending with 50 ps (30 ps for $u_{wall} = 4$ km/s) on the right. The symbol $\times$ denotes the temperature and position of the compressed, unreacted material immediately behind the shock front. $u_{wall} = $ (A) 3 and (B) 4 km/s.
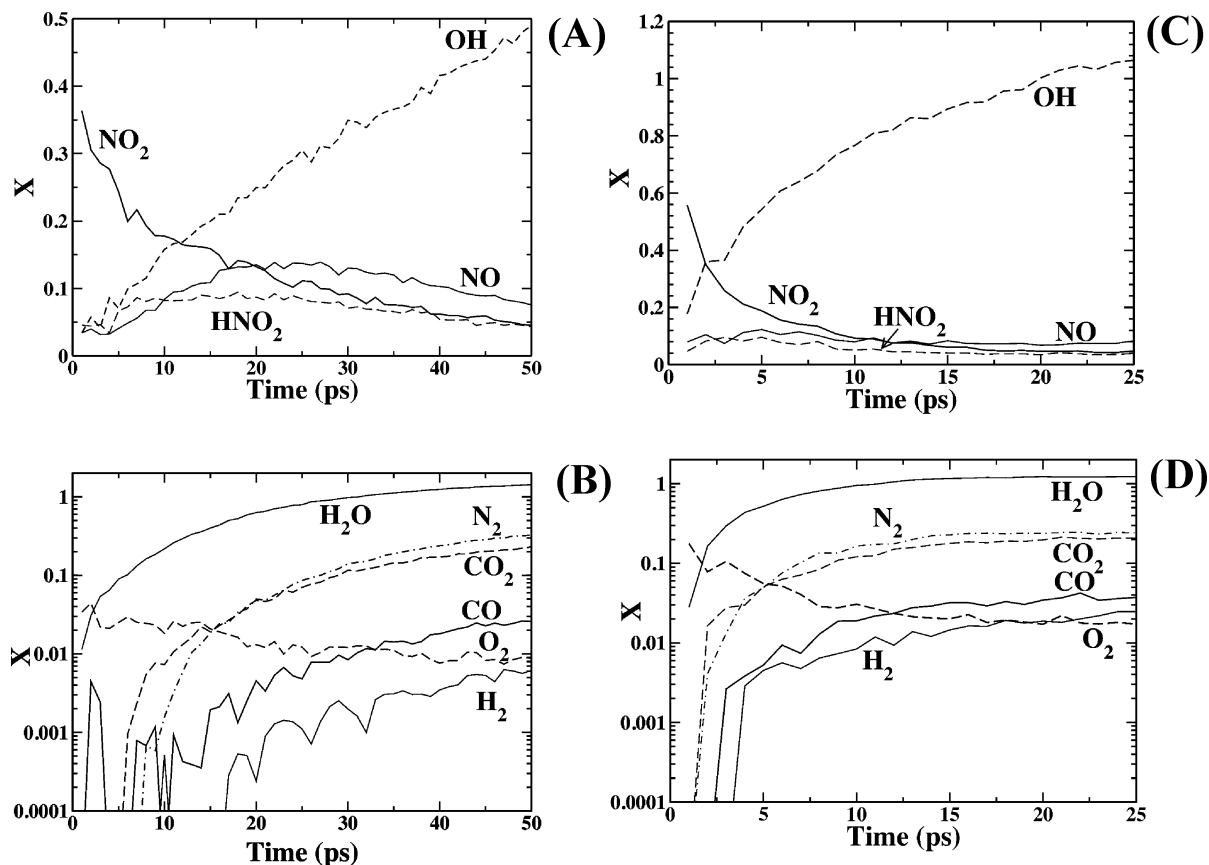
Figure 7. Primary and secondary products by time (normalized by PETN reacted). u_{wall} = (A and B) 3 and (C and D) 4 km/s.
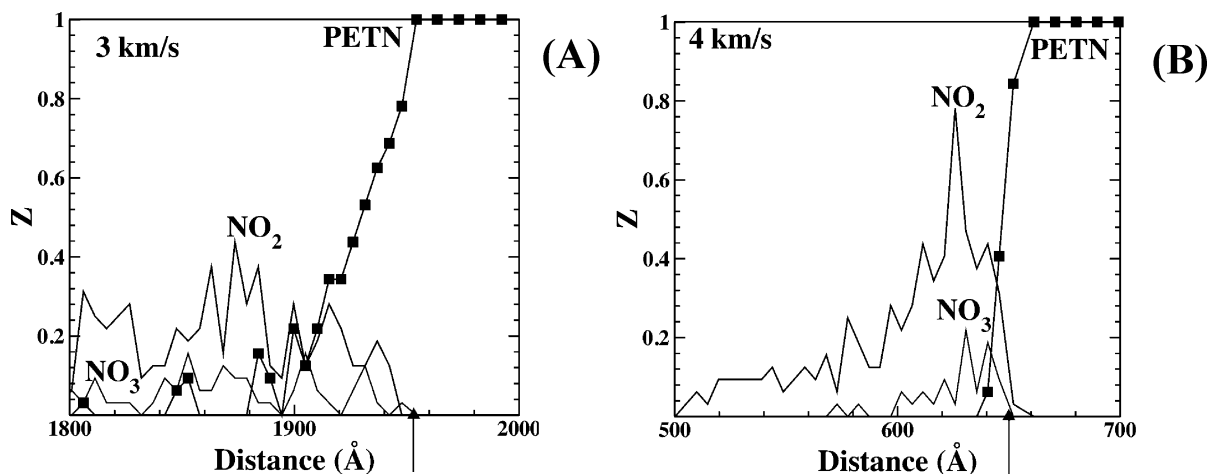

Figure 8. Initial products proposed in the literature. (A) u_{wall} = 3 km/s at 50 ps. (B) u_{wall} = 4 km/s at 15 ps. For clarity, zeros have not been plotted. Arrows indicate shock front positions determined from velocity. Squares indicate PETN; the solid dark gray line is NO_2; the light gray line is NO_3 for both parts.

not exceed it until about 50 ps. These results are reasonable considering that (a) these simulations are of a single crystal, not a porous solid, and (b) these simulations are overdriven and therefore do not have a steady detonation state.

The momentum equation[20] can be used to estimate the axial pressure at a steady state with mass velocity u_p behind the shock front:

$$P_{xx} = \rho_0 u_p U_s \qquad (3)$$

Using the data in Figure 3, ρ_0= 1.47 g/cm^3, and $u_p = u_{\text{wall}} =$ 3 or 4 km/s as appropriate, P_{xx} as a function of time can be estimated. At the end of the runs, the stronger shock has an estimated P_{xx} of approximately 52 GPa while the weaker shock is about 33 GPa. For comparison, profiles of the axial pressure determined directly from the simulation are plotted in Figure 4. While the pressure profiles show noise near the wall, the appropriate position for comparison with the estimation, the estimates are in reasonable agreement with the values obtained directly from simulation.

For the stronger shock, the axial pressure overshoots just behind the shock front before attaining a plateau value (see Figure 4B). This plateau value for the stronger shock does not appear to be increasing with time. In contrast, the weaker shock
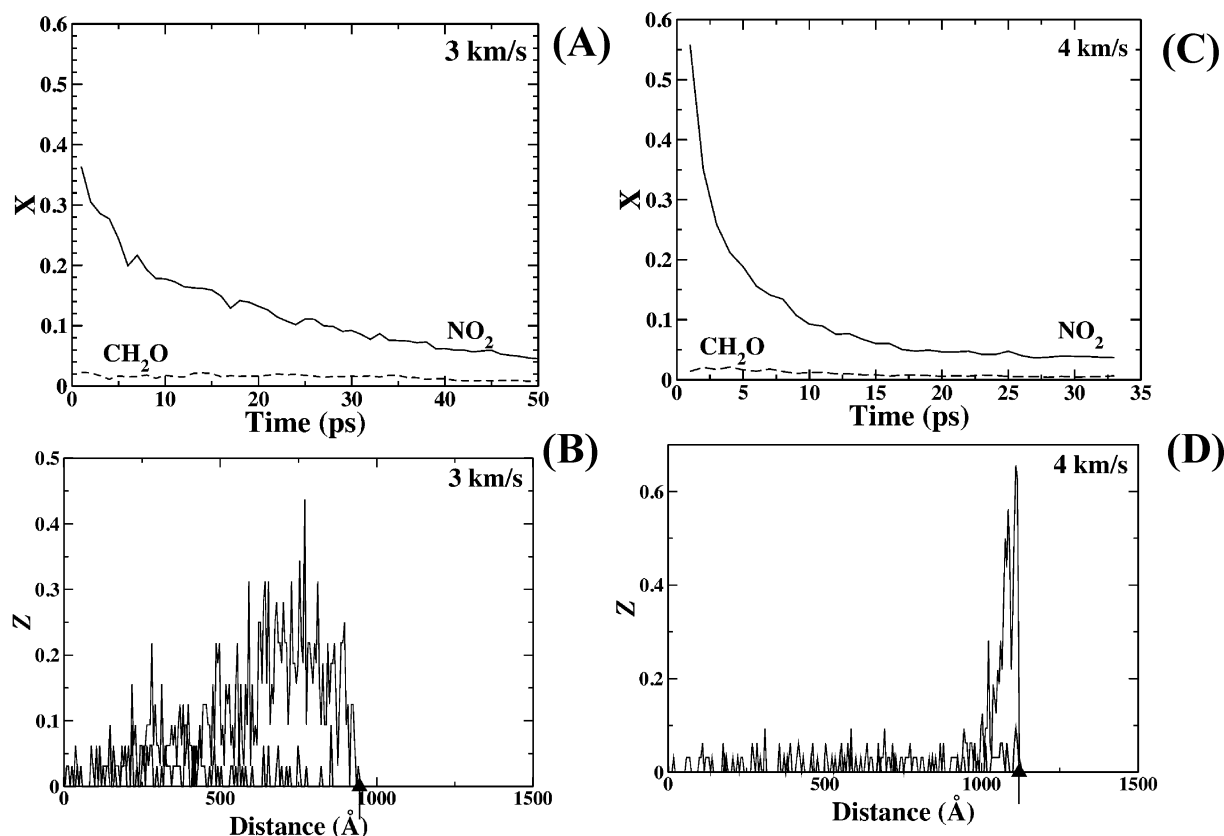
Shock Through a Single Crystal of PETN

J. Phys. Chem. B, Vol. 113, No. 40, 2009 **13147**

Figure 9. Examining the formation of formaldehyde. u_{wall} = (A and B) 3 and (C and D) 4 km/s. For the profiles B and D, the gray line is NO_2 and the black line is CH_2O. The shock front position is marked by the arrow. The profiles are calculated at 25 ps.

pressure (Figure 4A) appears to be increasing both in the shoulder near the shock front and farther behind the shock front. This result agrees with the slow increase over time of the axial pressure estimated near the wall from eq 3 based on the data in Figure 3.

For another comparison value, Green and Lee presented experimental data[19] using an acoustic method to measure the pressure at the Chapman−Jouguet (CJ) point. They report that at ρ_0 = 1.460 g/cm^3, P_{CJ} = 20.63 GPa and at ρ_0 = 1.532 g/cm^3, P_{CJ} = 21.05 GPa. A linear interpolation for ρ_0 = 1.47 g/cm^3 gives P_{CJ} = 20.7 GPa. The measured axial pressures are substantially above this P_{CJ} value because the systems simulated here are largely overdriven and are not fully reacted, thus still remaining at the von Neumann state. From the work of Yoo et al.,[3] detonation in the [100] direction occurs at input shock pressures near 31 GPa, the experimental CJ point for a single crystal, while a weaker shock at pressure of 23 GPa does not initiate a sustained detonation. In our simulations, the crystal behind the front of the strong shock wave is overdriven at well above that pressure, while the weakly shocked system has the input pressure near the wall close to that limit.

In contrast to pressure, which has noisy profiles that make determining trends of behavior with time difficult, the density profiles for both systems are smooth and show a definite trend as a function of time (Figure 5). The weakly shocked system shows a jump in density at the shock front that develops into a broad peak at times corresponding to the acceleration in the shock velocity. At all times, the strongly shocked system shows a sharp overshoot just behind the shock front followed by a relatively constant plateau. By the end of the simulation, the difference of densities at the spike top and near the wall reaches ∼12% relative to the wall density in the weakly shocked system and ∼7% for the strongly shocked system. As one may expect,

the strongly shocked system has a higher density (∼2.71 g/cm^3) near the wall than the weakly shocked system (∼2.44 g/cm^3). Both of these values are higher than the 2.39 g/cm^3 density at the experimental CJ point.[21]

The temperature behavior of the two systems is qualitatively different. From Figure 6, the weaker shock has a much smaller initial temperature jump than the stronger shock. The stronger shock system appears to have a plateau region in the temperature at long times while the temperature of the weaker shock system appears to still be increasing. These results are consistent with the shock velocity results because the stronger shocked system has reached a steady shock velocity by the end of the simulation time while the weakly shocked system is still accelerating.

For a single crystal of PETN shocked along the [100] direction, Yoo et al.[3] report an initial overshoot temperature of ∼5000 K with a steady state detonation temperature at CJ point of 4190 K for an impact velocity of 4.00 km/s and input shock pressure of 31.3 GPa. For the systems shown here, 5000 K is reached quickly at the impact face for the 4 km/s shock, with most of the compressed crystal reaching that temperature after 20 ps. The 3 km/s shock has a much lower temperature rise at the front and only reaches values of 4200 to 4300 K near the wall at approximately 45 ps.

In Figure 6A, the ×'s denote that the temperature of the compressed material immediately behind the shock front that has not yet begun to react. The temperature of the shocked, unreacted crystal appears to be about 1200 K after 5 ps with a noticeable gradual increase to ∼1500 K at 45 ps as the shock wave accelerates over time. The system shocked at 4 km/s reacts so quickly upon being compressed that no shocked but unreacted layer behind the shock can be clearly distinguished.

The greatest benefit of doing simulations with a reactive force field is that we can look at reactions directly through the evolution

of chemical species. Of primary interest are the product species seen in experiments. For ease of comparison, we define

$$X_i = \frac{\text{no. of } i \text{ molecules}}{\text{no. of PETN molecules reacted}} \qquad (4)$$

Plotting this value as a function of time as is done in Figure 7 allows us to track how far toward completion the reactions have gone. Both systems show the generally expected behavior. The primary products should have maxima as they form and then react away to secondary products. NO, NO_2, and HNO_2 show this behavior while OH continues to rise during the simulation time. The secondary products tend to increase with time and number of reacted PETN molecules as expected.

However, the systems show qualitative differences in their behavior. The strongly shocked system has little lag before secondary products appear, and by 17 ps, the system has little change in rate of production of several secondary products. These results are consistent with the idea that the shock front velocity accelerates due to the starting of exothermic reactions (resulting in secondary products) and then becomes constant when those reactions reach steady state. Also consistent with that idea is the behavior of the weakly shocked system, which shows a substantial lag in the generation of H_2, CO_2, and N_2, with a few of those molecules produced until about 15 ps, followed by steadily increasing production even at 50 ps.

We are not limited to looking merely at the total number of molecules. We can also see the progression of reaction through the crystal by looking at the spatial profiles of molecules. For convenience, we have defined

$$Z_i = \frac{\text{no. of } i \text{ molecules in a bin}}{\text{no. of initial PETN molecules in a bin}} \qquad (5)$$

where each bin initially contains 32 PETN molecules. Plotting in this way allows us to see more easily the relative rates of production of various chemical species.

Earlier in this paper, the idea was presented that the initial deceleration of the shock velocity for the weaker shock, which appears in Figure 4 prior to 15 ps, was related to the endothermicity of the NO_2 dissociation. While simulating thermal decomposition of PETN at constant temperature near the CJ point, Wu et al.[10] observed that formation of NO_2 was the most prevalent result of an initiation reaction, with formation of ONO_2 less likely. They found that initiation by breaking a C−C bond to produce an entire CH_2ONO_2 fragment also occurred, but those fragments were observed to form much less frequently than the other two moieties. Ng et al.[22] showed experimentally that the primary initiation pathway was dependent on method of initiation, with slow thermal reactions or low energy fracture producing a lot of NO_2, high-energy laser producing ONO_2, and high-energy fracture producing CH_2ONO_2.

Figure 8 shows concentration profiles of the products of the most likely pathways in the initiation region near the shock front. The reaction front for dissociating PETN molecules is sharp for the strong shock but is more diffuse for the weakly shocked system. However, in both cases, the large concentration of NO_2 indicates that the production of NO_2 is by far the most prevalent pathway with NO_3 production much lower and CH_2NO_3 production so low that only the occasional molecule is seen.

Figure 8 also shows that shock strength makes a difference in products formed. The stronger shock shows that NO_2
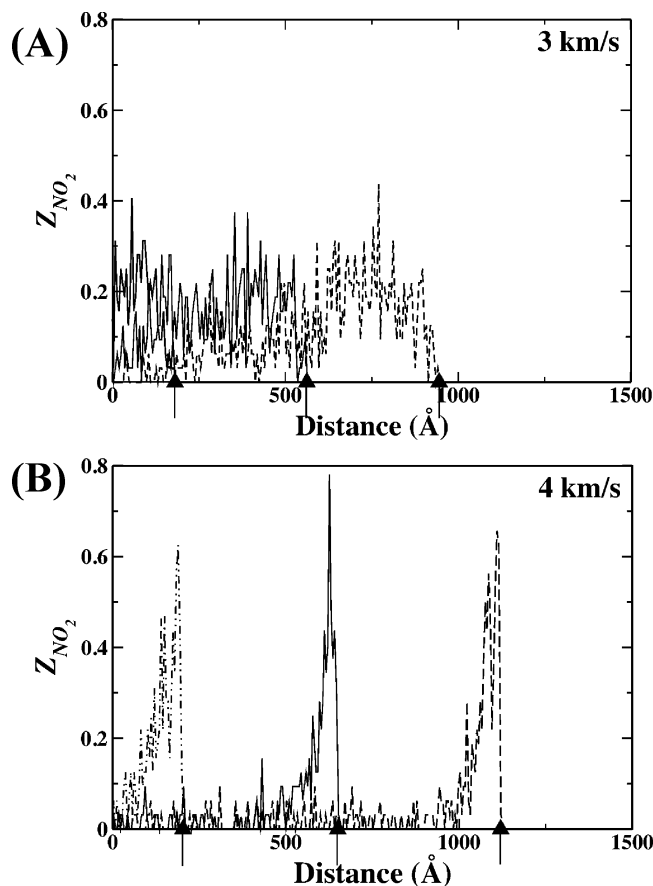

Figure 10. NO_2 molecules shown as a per initial PETN molecule basis. (A) $u_{wall} = 3$ km/s for times of 5, 15, and 25 ps (from the left). (B) $u_{wall} = 4$ km/s for times of 5, 15, and 25 ps (from the left). The arrows indicate shock front positions determined from the x-velocity.

production greatly outnumbers NO_3 production while the weaker shock also has NO_2 outnumbering NO_3, but to a lesser degree. The noise in Figure 8 for the PETN is some indication of the level of error associated with identifying the fragments.

The concentration of CH_2NO_3 may not be a good indicator of a C−C bond breaking as an initiation pathway in shocked PETN. Landerville et al.[8] performed first-principles MD simulations of binary collisions of PETN molecules to examine the effect of collision velocity on initial product formation. They found that PETN not only formed NO_2 as the first product but that often some CH_2O was formed as well. Wu et al.,[9] performing quantum mechanical MD simulations of binary collisions, also found CH_2O as a common product, although it was produced with lower frequency than NO_2. Thus, while CH_2NO_3 itself is not seen in appreciable quantities, CH_2O is another indicating specie that others have observed.

In Figure 9, the concentrations of NO_2 and CH_2O are compared. With our much larger simulations, we see that while formaldehyde does form near the shock front and eventually reacts away to secondary products, it is present in much smaller quantities than the NO_2. From thermal decomposition experiments at temperatures between 348 and 403 K, Ng et al.[23] postulated a reaction pathway for water that involved formaldehyde. However, we do not see evidence that this is the primary mechanism for either decomposition of CH_2O or formation of H_2O.

Having established that the primary initiation pathway is the formation of NO_2, further examination of NO_2 concentrations is warranted. Figure 10 shows some concentration profiles of
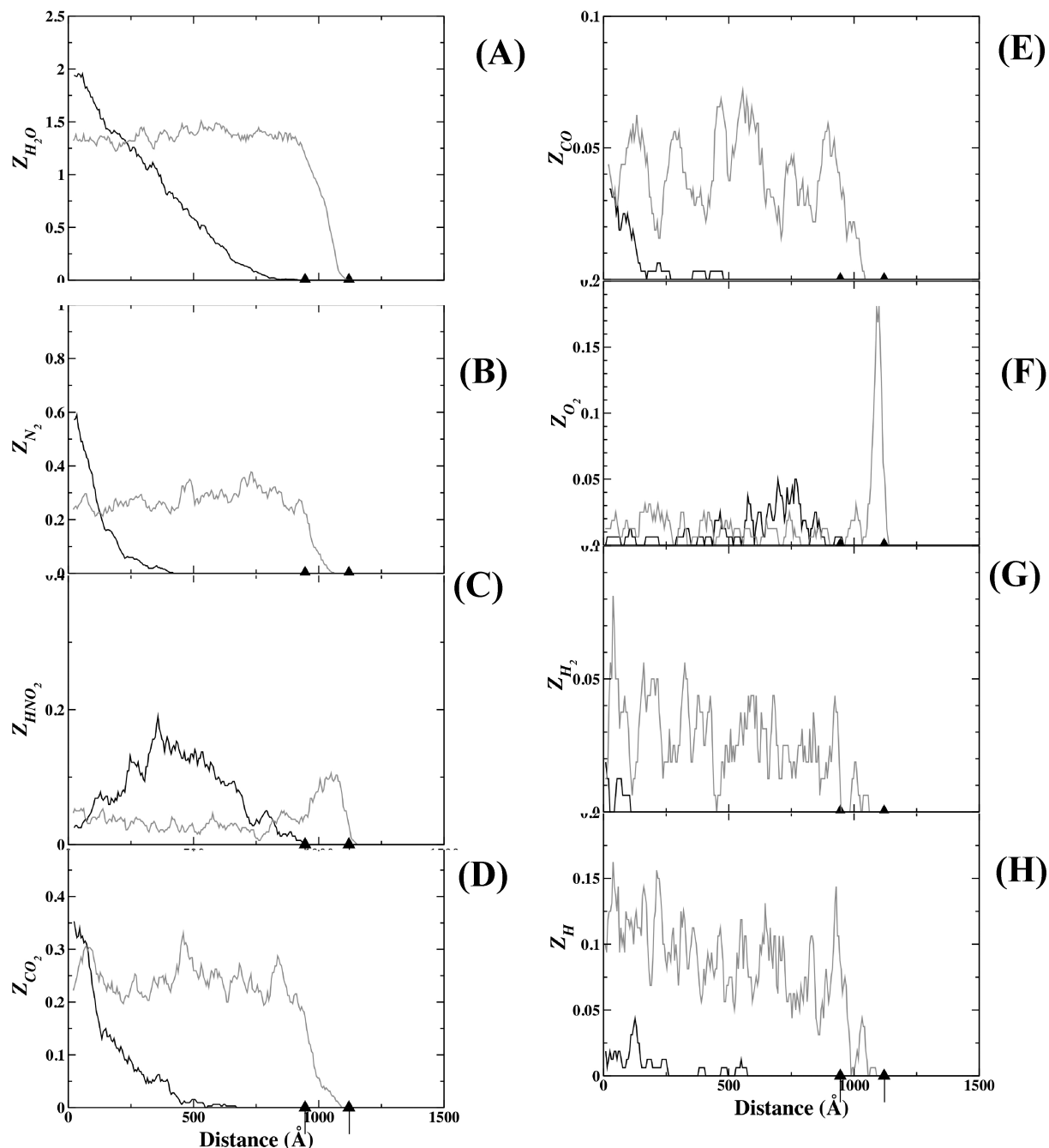
Shock Through a Single Crystal of PETN

J. Phys. Chem. B, Vol. 113, No. 40, 2009 **13149**

Figure 11. Secondary products at 25 ps. The black line is $u_{wall} = 3$ km/s; the gray line is $u_{wall} = 4$ km/s. (A) H_2O, (B) N_2, (C) HONO, (D) CO_2, (E) CO, (F) O_2, (G) H_2, and (H) H. The arrows indicate shock front positions determined from the *x*-velocity. A−E are ten-point running averages over each bin. F−H are five-point running averages.

NO_2 for both shock strengths. The strongly shocked system shows sharp peaks, indicating formation of NO_2 followed by fast reactions to other products. The weakly shocked system shows a much more diffuse peak, but it too shows further reaction after a reasonably short time.

Figure 11A−C show profiles of products related to the decomposition of NO_2, HONO, H_2O, and N_2. The weaker shock exhibits a substantial gap between the shock front position and the peak in NO_2 concentration. Consequently, the other molecules also show a substantial lag time between when the shock passed a particular material point and the initial rise in their concentration. In particular, the formation of H_2O in Figure 11A begins at a distance of about 750 Å from the wall, which corresponds to the peak in NO_2 concentration profile at 25 ps

in Figure 10A. This lag indicates a substantial delay in initiation of the exothermic formation of the secondary products and points toward a domination of endothermic NO_2 dissociation reactions during the first 10−15 ps after impact with the wall. As a result, the kinetic energy will be partially consumed by these reactions, leading to deceleration of the shock velocity as it appears in Figure 4 for the weaker shock.

Also presented in Figure 11 are several products that are of either high concentration or interest for other reasons. In all cases, as one might expect, the strongly shocked system shows reactions occurring much closer to the shock front than in the weakly shocked systems. These results correlate with the much sharper and higher temperature increase in the case of stronger shock, though it remains unclear if this is a cause or an effect.
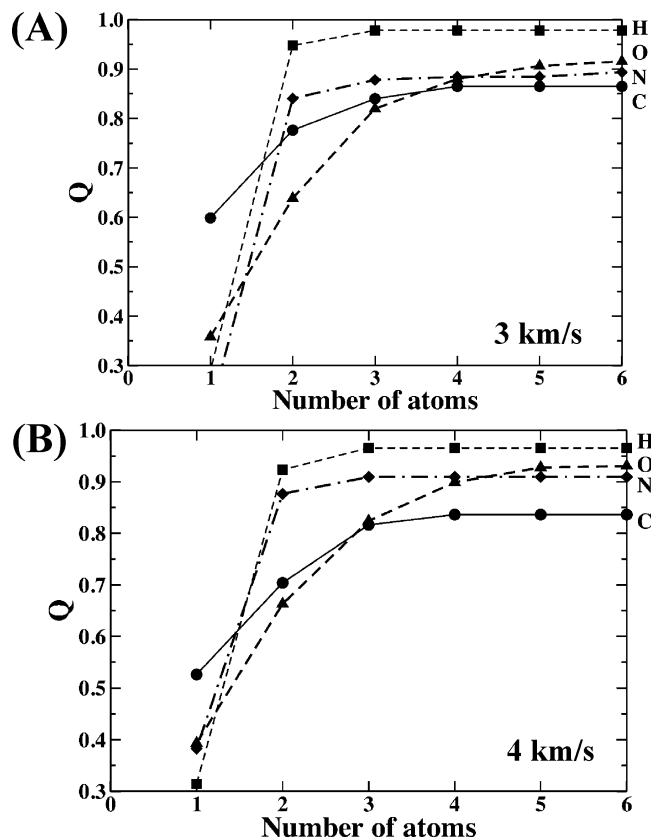
(A)

(B)

Figure 12. Fraction of atoms in clusters of N or fewer atoms (Q). u_{wall} = (A) 3 and (B) 4 km/s.

TABLE 2: Comparison of Simulation and Experimental Products at Long Times[a]

product	Z experimental (mol/mol PETN)	Z this work (mol/mol PETN)	
		3 km/s	4 km/s
CO_2	3.39 ± 0.04[25] 0.28[24]	0.3 ± 0.1	0.20 ± 0.06
CO	1.69 ± 0.03[25] 0.93[24]	0.07 ± 0.03	0.04 ± 0.04
N_2	2.00 ± 0.02[25] 0.07[24]	0.4 ± 0.1	0.23 ± 0.09
H_2	0.45 ± 0.01[25] 0.09[24]	0.03 ± 0.04	0.05 ± 0.05
H_2O	3.50 ± 0.05[25]	1.7 ± 0.2	1.1 ± 0.2
NH_3	0.038 ± 0.006[25]	0	0
CH_4	0.003 ± 0.001[25]	0	0
NO_2	0[25] 0.52[24]	0.02 ± 0.02	0.02 ± 0.02
NO	0[25] 2.11[24]	0.06 ± 0.04	0.1 ± 0.04
N_2O	0.42[24]	0.06 ± 0.04	0.03 ± 0.03

[a] The 3 km/s data is at 67 ps, and the 4 km/s data is at 33 ps.

To compare with experiment for the products at the end of the simulations, the profile data for approximately the 100 Å of the crystal nearest the piston were averaged to give product compositions. The resulting values were not found to depend on the choice of range within a few bins or the choice of time within a few picoseconds. Comparison to the classic results of Rideal and Robertson[24] on the decomposition of PETN in a closed volume at 483 K as well as with the results from Ornellas, Carpenter, and Gunn[25] of confined explosion in a bomb calorimeter is made in Table 2.

The simulated systems have some final product concentrations that are similar to the experimental results. The Rideal–Robertson results are similar to the results found here for CO_2 and are within the same order of magnitude for H_2. The Ornellas et al. results are similar to the ones here for NH_3, CH_4, and NO_2 with the same order of magnitude for the concentration of NO for the weaker shock.

Experimentally, the product distribution is known to depend on temperature[23] and energy loading conditions[22] so that experiments themselves under different conditions do not necessarily agree. With the simulated results still at high temperature so that dissociation is an issue (Figure 11G and H shows this effect for hydrogen) and the lack of a fully formed steady von Neumann spike, the simulated results should not agree exactly with experimental product distributions. In addition, many of the product concentrations relative to the number of PETN molecules reacted continue to increase with time (see Figure 7), which indicates that reaction has not run to completion.

The careful reader will note that Table 2 does not account for most of the atoms in the initial system. Several thousand compounds show up in the intermediary products, but most of these tend to exist for short times (femtoseconds), only have a few examples (<5), or are likely artifacts of the high density (e.g., clusters that consist of thousands of atoms). However, substantial fractions of the atoms (more than 50% even at the end of the simulation) exist in these compounds in the compressed crystal.

To alleviate the cluster artifacts due to high compression, a 100 Å slab of material adjacent to the piston at the end of each simulation was cut out and allowed to freely expand in the nonperiodic direction—the one that the shock wave had traveled along with this slab of materials lying far behind the shock front—for 0.64 ps for u_{wall} = 4 km/s and 0.95 ps for u_{wall} = 3 km/s. Over this short time, the material has little time to react, while the lower density allows for better identification of existing molecules.

To determine mean numbers of product molecules in these expanded samples, five configurations taken 10 fs apart were chosen near the end of the expanded simulation. The 4640 atoms nearest the piston (corresponding to five original unit cells in the shocked direction, which is approximately 50 Å of expanded material) were used. The top ten products by average number are shown in Table 3. Identification of most of the expected final products (H_2O, CO_2, CO, N_2) increase dramatically using this expansion technique, as has been observed for other shock simulations.[17] However, the lack of complete reaction and the very high temperature are reflected by the presence of several radical species (including HCO^+ that is not usually reported in terrestrial settings) and molecular oxygen.

More than 90% of the atoms in the expanded samples were located in small molecules that contain at least 100 instances during the averaging time. The list of these most common species contained 215 entries for u_{wall} = 3 km/s and 228 entries for u_{wall} = 4 km/s. Most of these species occur with a frequency of less than one per spatial averaging bin ($Z < 0.03125$). We define Q as the fraction of a particular element that exists in clusters containing N or fewer atoms of that element type. For just these persistent molecules, we have made a plot of Q versus number of atoms (Figure 12). The molecules are indeed small with most of the elements reaching a plateau of around three atoms. At least 85% of the original atoms for each element can be located in this manner with carbon the most likely element to be residing in short-lived, uncommon fragments.

Shock Through a Single Crystal of PETN

J. Phys. Chem. B, Vol. 113, No. 40, 2009 **13151**

TABLE 3: Top Ten Species by Average Number at the End of the Simulation

	3 km/s			4 km/s	
molecule	ave no. per bin	Z	molecule	ave no. per bin	Z
H_2O	66 ± 0.6	2.1 ± 0.02	H_2O	60 ± 0.5	1.9 ± 0.1
CO	24 ± 2	0.76 ± 0.06	OH^-	31 ± 2	0.96 ± 0.05
N_2	23 ± 0.3	0.72 ± 0.01	CO	26 ± 2	0.82 ± 0.5
OH^-	21 ± 1	0.64 ± 0.04	N_2	19 ± 0.4	0.60 ± 0.1
CO_2	20 ± 1	0.64 ± 0.04	CO_2	15 ± 1	0.47 ± 0.2
$HCOO^-$	13 ± 1	0.41 ± 0.04	NO	10 ± 0.6	0.31 ± 0.02
HCO_3^-	9.4 ± 0.5	0.30 ± 0.01	$HCOO^-$	7.5 ± 0.4	0.23 ± 0.01
HN_2^+	4.5 ± 0.3	0.14 ± 0.01	O_2	6.0 ± 0.4	0.19 ± 0.01
HCO^+	4.4 ± 0.3	0.14 ± 0.01	HCO_3^-	5.1 ± 0.6	0.16 ± 0.02
HNO	4.2 ± 0.2	0.13 ± 0.01	HCO^+	5.1 ± 0.3	0.16 ± 0.01

4. Conclusions

Using the reactive force field ReaxFF, MD simulations of pentaerythritol tetranitrate single crystals were performed. Each crystal, which consisted of a few hundred thousand atoms, was shocked along the [100] direction with either a 3 or 4 km/s piston. The shock front velocity for the simulations was tracked, and the two different shocks exhibited behavior that was qualitatively similar, but the weaker shocked system evolved much more slowly. Both systems showed an accelerating shock front during some part of the simulation. The strongly shocked system accelerated within a few picoseconds of the shock being applied, while the weakly shocked system had a long initial period of slight deceleration followed by a more rapid acceleration. By the end of the simulations, the shock front for the strongly shocked system had appeared to stop accelerating, while the shock front for the weakly shocked system was still accelerating.

Thermomechanical properties of the systems were tracked for positions behind the shock front. For properties other than temperature, the strongly shocked system exhibited a peak just behind the shock front for most of the simulation. The weakly shocked system developed a broad peak during the later parts of the simulation.

The chemical reactions that occurred were also tracked as a function of time and position behind the shock front. As one may expect, reactions occurred much more quickly in the strongly shocked system; however, the weaker shock exhibited similar behavior, after a delay and over a longer time period.

While agreement with previous experiments is not perfect, our results are reasonable and therefore can be used to gain some insight into the initiation mechanism for PETN. The most prevalent initiation pathway observed was the breaking of the $O-NO_2$ bond to yield NO_2. However, nonzero concentrations of NO_3, CH_2NO_3, and formaldehyde were also observed just behind the shock front, indicating that other pathways are also active. Farther behind the shock front, the concentrations of primary products steadily decreased, while secondary products increased. The final products show similarities to those found in experiments even though reactions were incomplete so that a direct comparison of product concentrations is not possible.

This work represents a significant step in using molecular simulations to directly investigate the initiation process in high explosives. Large-scale simulations using reactive force fields are now capable of studying systems that are approaching experimentally relevant sizes. Future work in this area will involve the effects of crystal orientation and different deformation mechanisms.

References and Notes

(1) Dick, J. J.; Mulford, R. N.; Spencer, W. J.; Pettit, D. R.; Garcia, E.; Shaw, D. C. *J. Appl. Phys.* **1991**, *70*, 3572.
(2) Dick, J. J.; Ritchie, J. P. *J. Appl. Phys.* **1994**, *76*, 2726.
(3) Yoo, C. S.; Holmes, N. C.; Souers, P. C.; Wu, C. J.; Ree, F. H.; Dick, J. J. *J. Appl. Phys.* **2000**, *88*, 70.
(4) Dick, J. J. *Appl. Phys. Lett.* **1984**, *44*, 859.
(5) van Duin, A. C. T.; Dasgupta, S.; Lorant, F.; Goddard, W. A. *J. Phys. Chem. A* **2001**, *105*, 9396.
(6) Oleynik, I. I.; Conroy, M.; Zybin, S. V.; Zhang, L.; van Duin, A. C. T.; Goddard, W. A.; White, C. T. *AIP Conf. Proc.* **2006**, *845*, 573.
(7) Nakano, A.; Kalia, R. K.; Nomura, K.; Sharma, A.; Vashishta, P.; Shimojo, F.; van Duin, A. C. T.; Goddard, W. A.; Biswas, R.; Srivastava, D. *Comput. Mater. Sci.* **2007**, *38*, 642.
(8) Landerville, A.; Oleynik, I. I.; Kozhushner, M. A.; White, C. T. *AIP Conf. Proc.* **2007**, *955*, 447.
(9) Wu, C. J.; Ree, F. H.; Yoo, C. S. *Prop. Explos. Pyrotechn.* **2004**, *29*, 296.
(10) Wu, C. J.; Manaa, M. R.; Fried, L. E. *Mater. Res. Soc. Symp. Proc.* **2007**, *987*, 139.
(11) GRASP is the general reactive atomistic simulation program developed at Sandia National Laboratories.
(12) Strachan, A.; van Duin, A. C. T.; Chakraborty, D.; Dasgupta, S.; Goddard, W. A. *Phys. Rev. Lett.* **2003**, *91*, 09301.
(13) van Duin, A. C. T.; Zeiri, Y.; Dubnikova, Y. F.; Kosloff, R.; Goddard, W. A. *J. Am. Chem. Soc.* **2005**, *127*, 11053.
(14) van Duin, A. C. T.; Zybin, S. V.; Chenoweth, K.; Zhang, L.; Han, S. -P.; Strachan, A.; Goddard, W. A. *AIP Conf. Proc.* **2006**, *845*, 581.
(15) Mortier, W. J.; Ghosh, S. K.; Shankar, S. *J. Am. Chem. Soc.* **1986**, *108*, 4315.
(16) Janssens, G. O. A.; Baekelandt, B. G.; Toufar, H.; Mortier, W. J.; Schoonheydt, R. A. *J. Phys. Chem.* **1995**, *99*, 3251.
(17) Strachan, A.; Kober, E.; van Duin, A. C. T.; Oxgaard, J.; Goddard, W. A. *J. Chem. Phys.* **2005**, *122*, 054502.
(18) Zybin, S. V.; Zhang, L.; van Duin, A. C. T.; Goddard, W. A., III Analysis of shock decomposition and sensitivity of energetic materials with ReaxFF molecular dynamic. *Proceedings of 13th International Detonation Symposium*, Norfolk, VA, July 2006.
(19) Green, L. G.; Lee, E. L. Detonation Pressure Measurements on PETN. *Proceedings of 13th International Detonation Symposium*, Norfolk, VA, July 2006.
(20) Cooper, D. W. *Explosives Engineering*; Wiley-VCH, Inc.: New York, 1996; p 182.
(21) Ree, F. H. *J. Chem. Phys.* **1984**, *81*, 1251.
(22) Ng, W. L.; Field, J. E.; Hauser, H. M. *J. Appl. Phys.* **1986**, *59*, 3945.
(23) Ng, W. L.; Field, J. E.; Hauser, H. M. *J. Chem. Soc., Perkin Trans.* **1976**, *6*, 637.
(24) Rideal, E. K.; Robertson, A. J. B. *Proc. R. Soc. (London) Ser. A: Math. Phys. Sci.* **1948**, *195*, 135.
(25) Ornellas, D. L.; Carpenter, J. H; Gunn, S. R. *Rev. Sci. Instrum.* **1966**, *37*, 907.